Journal of Biomedical Optics

SPIEDigitalLibrary.org/jbo

Artery phantoms for intravascular optical coherence tomography: diseased arteries

Charles-Étienne Bisaillon
Guy Lamouche

SPIE

Artery phantoms for intravascular optical coherence tomography: diseased arteries

Charles-Étienne Bisaillon and Guy Lamouche
Conseil National de Recherches Canada—site de Boucherville, 75 Boulevard de Mortagne, Boucherville, Quebec J4B 6Y4, Canada

Abstract. We propose and test various strategies for the creation of artery phantoms mimicking different kinds of diseased arteries when imaged by intravascular optical coherence tomography (IVOCT). We first review the method for making healthy artery phantoms. We then describe the procedure to fabricate diseased artery phantoms with intima thickening, lipid pool, thin-capped fibroatheroma, calcification, and restenosis (homogeneous and layered) after stent apposition. For each case, a phantom is fabricated, an IVOCT image is obtained, and the image is compared to that of a real artery. © *2013 Society of Photo-Optical Instrumentation Engineers (SPIE)* [DOI: 10.1117/1.JBO.18.9.096010]

Keywords: medical imaging; coherent optical systems; tissues; targets.

Paper 130388R received Jun. 5, 2013; revised manuscript received Aug. 2, 2013; accepted for publication Aug. 14, 2013; published online Sep. 10, 2013.

1 Introduction

The literature on optical imaging provides a wealth of different solutions for the fabrication of optical tissue phantoms.[1] Phantoms can serve several purposes in relation to many different technologies to investigate many different tissue structures. With the intensive development of biomedical optics, new phantoms are continuously needed and are thus continuously being developed.

One niche for the development of new optical phantoms is to mimic tissues with complex structures having different optical properties.[2,3] Phantoms that realistically mimic tissues with healthy and diseased conditions are important tools for the validation and the standardization of optical imaging technologies.[4] Additionally, they provide valuable tools for training personnel to use a system or to interpret data, for demonstrating technology capabilities, and for developing new hardware, new software, and new procedures.

The ability of intravascular optical coherence tomography (IVOCT) to visualize various types of healthy and diseased arterial tissues has been demonstrated in numerous publications including the Consensus Report produced by the International Working Group for Intravascular OCT Standardization and Validation.[5] This report also highlights the need for artery phantoms to pursue the development of IVOCT. Recently, a review was also published for tissue mimicking phantoms specifically used with optical coherence tomography.[6] However, arteries have complex tubular and multilayer geometries and can present various other inhomogeneities. To our knowledge, no method has yet been presented to fabricate tubular phantoms with such complexity.

In a previous publication, we introduced a method for the fabrication of healthy coronary artery phantoms.[7] These phantoms are multilayer tubular structures fabricated with a silicone matrix. They mimic the IVOCT signal from the artery layers, offer mechanical elasticity similar to arteries for small deformations and provide long-term stability.

In this paper, we present a further development of the fabrication method to provide diseased artery phantoms. In Sec. 2, starting from a brief review of the method to fabricate healthy artery phantoms, we present the guidelines of the more elaborate method to fabricate diseased artery phantoms. In Sec. 3, we describe the IVOCT system used to characterize the phantoms. Finally, in Sec. 4, we demonstrate the detailed steps to fabricate phantoms with specific pathologies: intimal thickening, lipid pool, thin-capped fibroatheroma (TCFA), calcification, and homogeneous and layered restenosis after stent apposition. In Sec. 4, we also present, for each type of pathology, an IVOCT image of a phantom measured with our IVOCT system and compare it to the IVOCT image of a real diseased artery from the literature. Our overall goal is to demonstrate the efficiency and versatility of our method for the fabrication of complex diseased artery phantoms.

2 Fabrication

2.1 *Healthy Artery Phantoms*

Our design of artery phantoms relies on the fact that, for a homogeneously scattering medium, the amplitude of the OCT signal depends on the backscattering from the medium and decays in depth with its total attenuation.[8] In our phantoms, a scattering agent provides the backscattering and also a part of the attenuation. The total attenuation is adjusted by the addition of an absorbing agent. Different optical signatures of tissues can be mimicked by mixing different concentrations of each agent in a transparent matrix.

In our method, alumina powder (Al_2O_3) provides the backscattering and carbon black provides the additional attenuation, when needed. A detailed characterization of the variation in optical properties with the alumina and carbon black concentrations is provided in Ref. 7. The particle sizes were observed with a scanning electron microscope. The alumina shows

Address all correspondence to: Guy Lamouche, Conseil National de Recherches Canada—site de Boucherville, 75 Boulevard de Mortagne, Boucherville, Quebec J4B 6Y4, Canada. Tel: 450-641-5198; Fax: 450-641-5106; E-mail: guy.lamouche@cnrc-nrc.gc.ca

0091-3286/2013/$25.00 © 2013 SPIE

approximately spherical particles with an average size of 300 nm. The carbon black also shows spherical particles with an average diameter of 50 nm. They are mixed in a transparent silicone matrix. This combination of inorganic components insures long-term durability, as no change of OCT signal amplitude and attenuation was observed over a period of 13 months on our set of phantoms.[7] The silicone is a mixture of the commercial room temperature vulcanizing silicone Sylgard 184 with pure poly(dimethylsiloxane) (PDMS) (Fluid 200, 50 cst, Dow Corning). Adjusting the ratio of PDMS, Sylgard resin and Sylgard reactive change the elasticity of the resulting silicone.[6,9] A ratio of 15 : 15 : 1 in PDMS:resin:reactive is normally used, which approximates the elasticity of porcine arteries for low deformations while resulting in a fully polymerized silicone with a smooth surface.

Healthy arteries are composed of three layers: the intima, the media, and the adventitia. These three layers can be discriminated by IVOCT since they have different optical properties. Within each layer, we consider that the optical properties are homogeneous. Therefore, healthy artery phantoms are made of three layers with three mixtures of different concentrations of alumina and carbon black in a silicone matrix.

The concentrations required to mimic the optical properties of each layer can be obtained using a calibration process detailed in our previous publication.[7] We review here the two main steps of the calibration process.

In the first step, we measured the amplitude and attenuation of the OCT signal on calibration phantoms with different concentrations of alumina and carbon black. The calibration phantoms were fabricated in puck shapes, which facilitated the calibration measurements. The calibration provided curves relating the OCT amplitude and total attenuation to the concentrations. In the second step, we measured the OCT amplitude and total attenuation for each layer of coronary arteries. We selected porcine arteries because of their easy availability. Measurements on seven different arteries, divided into several sections, gave statistical distributions of the OCT amplitude and total attenuation for both the media and the adventitia. No value was obtained for the intima of porcine arteries since the intima was too thin.

The properties measured from porcine arteries showed an important variability. Therefore, the effectiveness of the calibration process was demonstrated mimicking the OCT signal from a specific artery. For that particular artery, the signal from the media was mimicked using concentrations of 14 mg/ml of alumina and 0.5 mg/ml of carbon black. For the adventitia, the signal was mimicked with 60 mg/ml of alumina.[7] Since, the intima has normally higher scattering than the media, but also has lower attenuation, a concentration of 20 mg/ml of alumina, without carbon black, was chosen to qualitatively approximate its optical properties.

The most novel aspect of the method is the fabrication of phantoms in the form of multilayer tubes. The process consists of the successive deposition and polymerization of the layer mixtures on a lathe setup. This setup is presented in Fig. 1 and the different steps of the fabrication process were described in detail in our previous publication.[7] The setup mainly consists of a shaft rotating near a blade, with the phantom material being deposited with a syringe. The distance between the blade and the shaft adjusts the layer thickness, allowing thicknesses as thin as approximately 30 μm. That method of adjusting layer thicknesses provides much more freedom than a molding process.

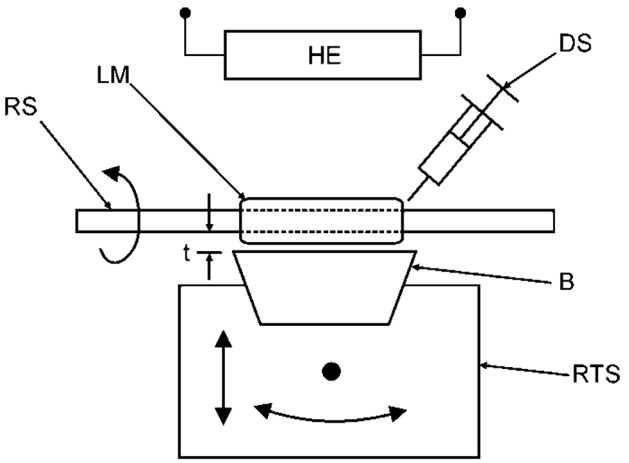

Fig. 1 Lathe setup for artery phantom fabrication. RS, rotating shaft; LM, layer mixture; DS, deposition syringe; B, blade; RTS, rotation and translation stage; HE, heating element; t, thickness.

2.2 *Diseased Artery Phantoms*

Diseased arteries have more complex structures than healthy arteries. In atherosclerotic lesions, the intima layer (or fibrous tissue) is thickened and often surrounds, or covers, different features such as calcifications, lipid pools, stents, etc. These features have distinctive optical properties that make them often observable in IVOCT images. In this section, we outline our more elaborate method to fabricate phantoms of diseased arteries.

To obtain an asymmetric thickened intima, we proceed as described in the previous section but with a cavity machined in the shaft that supports the phantom. Filling the cavity creates a reduction of the phantom lumen related to the lesion. Whenever lesions are more complex than simple intima thickening, we include additional materials within the cavity to mimic the additional structures.

Like for healthy artery phantoms, diseased phantoms are built from the inside out. Figure 2 illustrates the different steps involved in the phantom fabrication for the specific case of an eccentric plaque with an inclusion. Figure 2(a) shows a shaft with a flat groove machined to locate the eccentric lesion. The fabrication of the phantom starts with the deposition of the intima mixture to create the cap of the plaque [Fig. 2(b)]. At this point, the rotation of the shaft has not yet started. Then, the inclusion mimicking a specific feature is put in place [Fig. 2(c)] and covered with intima mixture to fill the groove [Fig. 2(d)]. The rotation of shaft is then started, and the phantom fabrication is continued with the application of the intima mixture on the full length of the phantom [Fig. 2(e)] followed by the application of the media [Fig. 2(f)] and adventitia [Fig. 2(g)] mixtures. Once the phantom is completed, the rotation is stopped, and the phantom is removed from the shaft [Fig. 2(h)]. The elasticity of the silicone greatly facilitates the last step since it allows stretching the lesion over the shaft. Even if presented for a specific case, these fabrication steps are representative of the general method. Different artery lesions can be mimicked with slight modifications to this fabrication method.

The goal of this paper is to demonstrate the efficiency and versatility of this method by fabricating IVOCT phantoms of various types of plaque and comparing IVOCT images of the phantoms to IVOCT images of diseased arteries. Since

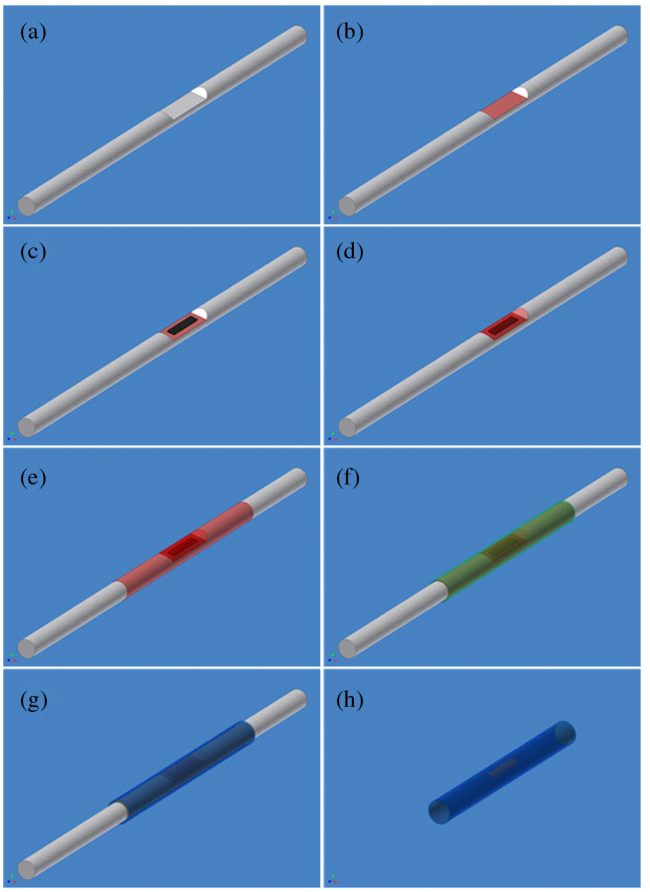

Fig. 2 Different steps for fabrication of an artery phantom mimicking an eccentric plaque structure with an inclusion. Steps are detailed in the text.

the optical properties of plaque structures are not yet well documented in the literature, the optical properties were empirically adjusted to qualitatively mimic the distinct IVOCT signature of each type of plaque. In doing so, we relied on the calibration performed for phantoms of healthy arteries to obtain the optical properties of the media and adventitia layers. For the intima, a mixture of 20 mg/ml was used to mimic a layer with high signal and low attenuation. That signature is the same for fibrous tissue. Because no characterization has been performed to differentiate between intima and fibrous tissue, their properties were considered identical and they were mimicked by the same mixture.

3 OCT Imaging

We performed IVOCT imaging to demonstrate how the phantoms efficiently mimic different pathologies found in coronary arteries. Images were acquired with a custom-built IVOCT system. The system has been described in detail in a previous publication.[10] Briefly, the swept-source OCT (SS-OCT) system uses a Santec source (Aichi, Japan) sweeping at a rate of 30 kHz over 108 nm around a wavelength of 1.33 μm. It provided an experimentally measured IVOCT resolution of 15 μm. The interferometer and electronic components are commercialized by Novacam Technologies (Pointe-Claire, Canada). The IVOCT system also used custom-built catheter probes coupled to a custom-built rotation and pullback unit. For phantom imaging, the probe rotated within a polymer sheath filled with water. The probe and phantoms were immersed in water to reduce the refractive index gaps between the lumen of phantoms and both the polymer sheath and phantom material. The images presented in the next section were selected from pullback measurements. The measurements were performed at a rate of 20 frames/s with 1500 lines per frame and a pullback speed of 2.0 mm/s.

4 Phantom Descriptions

In this section, we present IVOCT images of artery phantoms mimicking different pathologies. Fabrication strategies specific to each phantom are described in relation to the general fabrication steps described in Sec. 2.2. The IVOCT images of phantoms are compared to the IVOCT images of real human arteries. The latter images were extracted from a review on the IVOCT by Kim et al.[11] In this review, there is not much information about the system used to acquire these images. It is nevertheless reasonable to assume that the sepia-like images are presented using a logarithmic scale. The images of our phantoms acquired with our SS-OCT system are also presented using a logarithmic scale, but with a yellow-tone colormap.

4.1 *Concentric Intimal Thickening*

When imaged with IVOCT, both intimal thickening and fibrous plaque produce a homogeneous strong signal with weak attenuation.[5] In some arteries, the lumen area can be reduced by an even distribution of plaque around the vessel wall, resulting in nearly concentric structures. To create a concentric structure, we used a shaft slightly different from the one shown in Fig. 2(a). In this concentric case, a uniform reduction in diameter was machined within a certain region along with the shaft axis. A schematic of the shaft is shown in Fig. 3. A phantom mimicking concentric intimal thickening was fabricated with a shaft having a 3 mm nominal diameter, with a reduction to 2 mm over a length of 15 mm. We mimicked only intimal thickening, therefore no inclusion was used. The phantom fabrication was initiated by directly filling the region of reduced diameter with the intima mixture; then it was pursued by depositing the material over the full length of the phantom to complete the intima layer. Subsequent layers were finally deposited as described previously.

An IVOCT image of a human artery [Fig. 4(a)][11] is compared to the IVOCT image of the phantom [Fig. 4(b)]. The intima layer is much thicker in the phantom than in the artery; this reduces the visibility of the subsequent layers in the phantom. Nevertheless, our phantom provides the clear signature of intimal thickening.

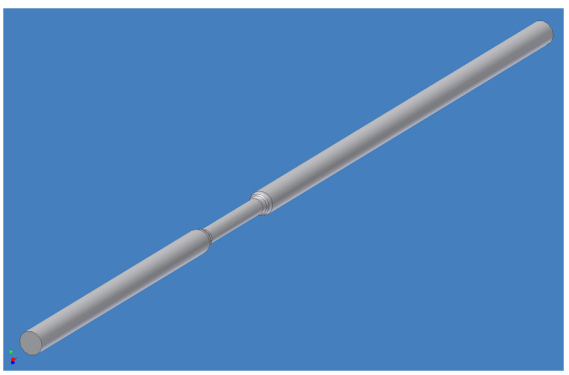

Fig. 3 Schematic of shafts used for the fabrication of concentric plaques.

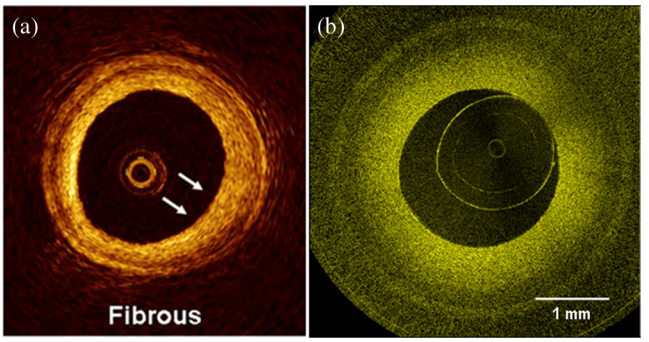

Fig. 4 Intravascular optical coherence tomography (IVOCT) images of (a) an artery with concentric intima thickening (reproduced from Ref. 11 with the permission from Springer) and (b) an artery phantom mimicking concentric intima thickening.

4.2 *Lipid Pool*

In OCT images, a lipid pool is recognized as a homogeneous signal-poor region with diffuse boundaries. It was demonstrated that the high scattering and high attenuation from lipids cause that particular signature.[12] The high scattering creates a diffuse border with the surrounding high scattering from intima, and the high attenuation causes the signal to decay rapidly, which casts a shadow of poor signal.

To fabricate a phantom that mimics a lipid plaque, an inclusion with high scattering and high attenuation was embedded in the phantom. The inclusion was fabricated separately and introduced in the intima cavity during step 2(c) of the fabrication process in Sec. 2.2.

A phantom was fabricated over a shaft of 3.175-mm diameter with a flat groove machined 1-mm deep over a length of 11.5 mm. The inclusion was a rectangular slab of polymerized silicone mixture. The inclusion mixture contained 20 mg/ml of alumina, the same alumina concentration as in the intima mixture; this insured diffuse boundaries. The inclusion mixture also contained 0.8 mg/ml of carbon black to increase the attenuation and create the shadow of poor signal. The formulation of silicone matrix for the lipid inclusion was the same as for artery layers (15:15:1, PDMS:resin:reactive).

Figure 5(a) shows a typical OCT image of human artery with a lipid pool.[11] Figure 5(b) presents the IVOCT image of the artery phantom mimicking a lipid pool. Our artery phantom provides the clear signature of a lipid pool: a signal-poor region with diffused boundaries.

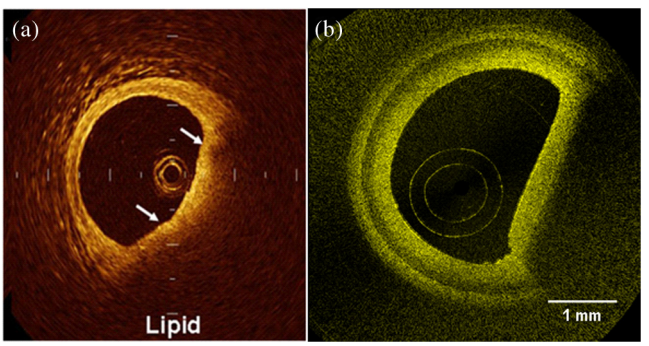

Fig. 5 IVOCT images of (a) an artery with a lipid plaque (reproduced from Ref. 11 with permission from Springer) and (b) an artery phantom mimicking a lipid plaque.

4.3 *Thin-Capped Fibroatheroma*

The TCFA is defined as a fibrous cap with the thickness thinner than 65 μm (as measured by histology) overlying a necrotic core. In IVOCT, the differentiation between necrotic cores and lipid pools is not yet fully characterized. Both are observed as a signal-poor region with diffuse borders. However, some studies have indicated a "fast signal drop-off" for necrotic cores, suggesting a higher attenuation.[5]

The process for fabricating a phantom with a TCFA was very similar to the process for fabricating a phantom with a lipid pool. An inclusion representing the necrotic core was fabricated separately. The main difference resided in the cap thickness. That thickness was adjusted by initially depositing a defined volume of intima mixture leading to a specific cap thickness since the size of the shaft cavity is known. Precision on the volume was obtained by measuring and depositing the volume with a micropipette.

Figure 6(a) presents an image of a lesion identified as a TCFA[11]. On the upper right quadrant, a thin cap covers a necrotic core. A lipid pool is also visible besides the TCFA.

A phantom mimicking the combined TCFA and lipid pool was fabricated with two adjacent inclusions made of two different mixtures. The necrotic core mixture was composed of 20 mg/ml of alumina and 2.0 mg/ml of carbon black. That carbon black concentration creates the larger signal drop-off. The attenuation of this mixture may be exaggerated, but this choice was made to accentuate the distinction from the cap, highlighting the cap thinness. The lipid pool mixture was composed of 20 mg/ml of alumina and 0.8 mg/ml of carbon black, as in Sec. 4.2. That particular concentration of carbon black was chosen to provide more light penetration in the lipid part relative to the necrotic core, insuring the differentiation of both structures.

Once the inclusion was fabricated, the phantom was constructed following the steps described in Sec. 2.2. A 3.175 mm shaft with a 1-mm deep and 11.5-mm long flat groove supported the phantom. The groove had a 2.95-mm width, and therefore, the 2.0 μl of intima mixture deposited with the micropipette gave a 59 μm cap thickness.

Figure 6 shows both the IVOCT image of a real artery [Fig. 6(a)][11] and an IVOCT image of the phantom [Fig. 6(b)]. On the top part of both lesions, there is a "fast signal drop-off" and a thin cap of about 60 μm, which qualifies both for a TCFA. On the bottom part of both lesions, the scattering decreases more slowly than for TCFA, and this corresponds to a lipid pool.

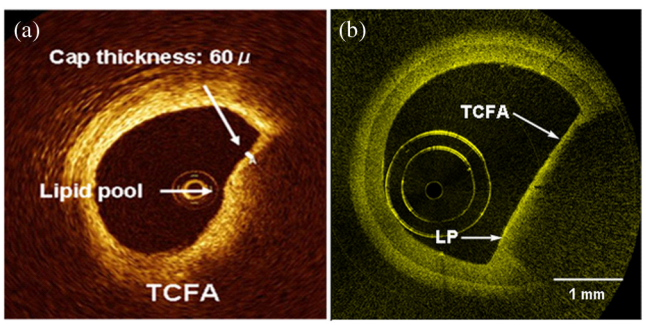

Fig. 6 IVOCT images of (a) an artery with a TCFA and a lipid pool (reproduced from Ref. 11 with permission from Springer) and (b) an artery phantom mimicking a TCFA and a lipid pool.

4.4 *Calcification*

Large calcifications are identified in IVOCT as regions of poor signal, with a low attenuation and well-delineated boundaries.[5] The signal from calcification can also be heterogeneous, with regions of mixed poor and high signal. Mechanically, studies demonstrated that the calcified tissue is on average stiffer than other types of plaques.[13,14]

To fabricate a phantom mimicking a calcification, we used an inclusion made with stiff material, with low backscattering, and low attenuation, but providing a heterogeneous signal. A stiff calcification was obtained with a polyurethane matrix. The mechanical properties of the polyurethane were not calibrated to the value of the real calcification. Polyurethane was used mainly to demonstrate that a stiffer, foreign material (not silicone) could also be used to create hard inclusions. Furthermore, transparent polyurethane (TechnoCast 3284, Polymères Technologies, Saint-Hyacinthe, Canada) allowed us to adjust the optical properties of the inclusion freely with additives. Polyurethane mixtures were prepared with the same method as for the silicone mixtures: by adding particles to the liquid resin, sonicating for 5 h, and adding the hardener for polymerization.[7]

A calibration was performed by measuring the OCT amplitude and the attenuation as a function of alumina concentration in a polyurethane matrix. The detailed results of that calibration are not given here. As an indication, 10 mg/ml of alumina in polyurethane provided roughly the same OCT amplitude as 3 mg/ml of alumina in silicone, but provided attenuation approximately 50% larger.

To fabricate the phantom, a polyurethane inclusion was molded in the shape of a half cylinder. Heterogeneous signal for the calcification inclusion was obtained by slightly mixing two different alumina/polyurethane mixtures. The two mixtures had concentrations of, respectively, 5 and 15 mg/ml of alumina in polyurethane. No carbon black was used since calcifications show low attenuation. After the preparation of the calcification inclusion, the phantom was constructed on the 3.175 mm shaft with a 1-mm deep groove, according to the process described in Sec. 2.2.

An IVOCT image of an artery with a calcification is presented in Fig. 7(a),[11] and an IVOCT image of the artery phantom with a calcified plaque is shown in Fig. 7(b). In both cases, we see a region of weak signal surrounded by very well-defined borders. The signal attenuation is small in both cases within the calcification since the outer borders of the calcification are clearly visible. In Fig. 7(a), the arrows point towards the calcified region. In Fig. 7(b), the arrows point within the calcified region, highlighting slight variations in the signal amplitude due to the heterogeneity of the calcification.

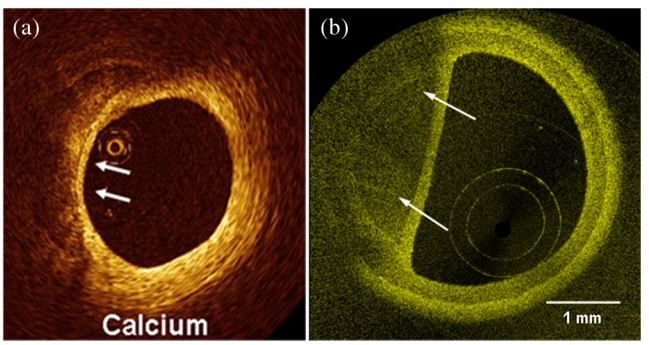

Fig. 7 IVOCT images of (a) an artery with a calcification (reproduced from Ref. 11 with permission from Springer) and (b) an artery phantom mimicking a calcification. In (a), the arrows point towards the calcified region. In (b), the arrows point within the calcified region, highlighting slight variations in signal amplitude due to the heterogeneity of the calcification.

4.5 *Stent Restenosis*

The IVOCT community has identified great potential for the IVOCT technology to assess stent apposition and to characterize strut coverage.[5] Stent struts are identified in IVOCT images by the strong reflection from their metallic surface. Because the metallic struts are opaque to light, they also cause discernible shadows that mask deeper tissue. Restenosic tissue covering the struts can either be signal rich or signal poor, and can have homogeneous, layered, or heterogeneous structures.[15] Homogeneous restenosis have uniform optical properties; layered restenosis show concentric layers with an inner high signal layer and an outer low signal layer; whereas heterogeneous restenosis show high signal regions and low signal regions that are not concentric. We have fabricated phantoms that mimic both homogeneous and layered restenosis after stent apposition. Heterogeneous restenosis will be the object of future work.

Phantoms with stent restenosis were constructed on shafts with rotational symmetry, i.e., either with or without a localized diameter reduction (see Fig. 3). The fabrication process was very similar to the one described in Sec. 2.2. The inclusions were actual stents deployed to their nominal diameter. Phantom fabrication began with the deposition of a mixture mimicking restenotic tissue for the homogeneous restenosis case. It began with the deposition of several mixtures for the various layers in the layered restenosis case. The layers thicknesses were adjusted to reach the nominal diameter of the stent. The stent was then slid over the cylindrical structure and the phantom fabrication pursued with the usual deposition of the three layers, thus embedding the stent.

The phantom of homogeneous restenosis was built around a shaft of 3-mm diameter, with a local reduction to 2.5 mm over a length of 15 mm. The strongly backscattering restenotic tissue was mimicked by a mixture of 20 mg/ml of alumina in silicone, the same mixture as for the intima layer. The stent embedded in the phantom was a 3.0×15 mm NIR Royal (Boston Scientific/Scimed, Inc., Maple Grove, Minnesota).

Figure 8(a) shows an IVOCT image of a real artery with a homogeneous stent restenosis.[11] Figure 8(b) shows an IVOCT image of the phantom with a homogeneous stent restenosis. In both cases, the optical properties of the restenotic tissue do not vary throughout the layer. The stent struts are clearly visible all around the two diameters, providing both strong signal amplitudes and discernible shadows. In the phantom image, we also observe the outer media and adventitia layers.

The process for the fabrication of the layered stent restenosis phantom was the same, except that the two restenotic tissue layers were fabricated from two different mixtures: the inner layer with a high scattering mixture and the outer layer with a low scattering mixture. The phantom was built around a normal cylindrical shaft with 2-mm diameter. The mixtures mimicking the inner and outer layers contained 20 mg/ml and 7.5 mg/ml of alumina, respectively. The stent was again a 3.0×15 mm NIR Royal (Boston Scientific/Scimed, Inc., Maple Grove, Minnesota).

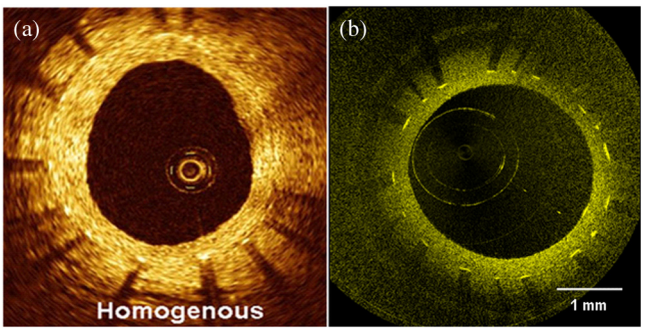

Fig. 8 IVOCT images of (a) an artery with a homogeneous restenosis (reproduced from Ref. 11 with permission from Springer) and (b) an artery phantom with a homogeneous restenosis.

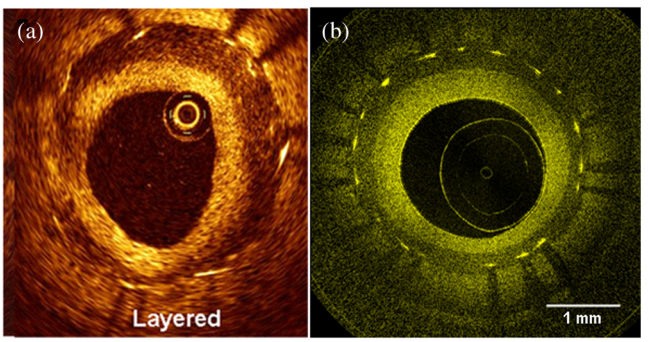

Fig. 9 IVOCT images of (a) an artery with a layered restenosis (reproduced from Ref. 11 with permission from Springer) and (b) an artery phantom with a layered restenosis.

Figure 9(a) shows an IVOCT image of a real artery with a layered stent restenosis.[11] Figure 9(b) shows an IVOCT image of the phantom with a layered stent restenosis. The two layers with different optical properties are clearly identified in both the real artery and the phantom. The media and the adventitia can again be seen in the phantom image.

5 Conclusion

In this paper, we have presented different strategies implemented to fabricate durable phantoms of diseased coronary arteries. These strategies complement the method for the fabrication of healthy coronary arteries published in a previous paper.[7] These strategies were demonstrated by the fabrication of artery phantoms mimicking: concentric intima thickening, calcification, lipid pool, TCFA, and homogeneous and layered restenosis after stent apposition. Mimicking all these conditions with a single method to fabricate phantoms demonstrated the efficiency and versatility of the fabrication method. The optical properties of the materials used to mimic these diseases were defined empirically providing a significant qualitative signature. A few groups have initiated the quantitative characterization of plaque optical properties.[12,16–18] However, the literature is not extensive enough, and values obtained show some discrepancies between publications. A calibration of the optical properties of plaque components with the same method as the calibration of healthy artery layers[7] is the object of future work. It would enhance the value of these diseased artery phantoms. Future work also includes the replication of other pathologies such as heterogeneous stent restenosis, red and white thrombosis, macrophage infiltration, intimal vasculature, dissections, cholesterol crystals, etc.

Acknowledgments

The authors would like to thank Jennifer Robb for her help in phantom fabrication. The authors also thank Marc Dufour and Bruno Gauthier for numerous helpful discussions. The authors acknowledge the financial support provided by the National Research Council Canada through the Genomics and Health Initiative. Images from human arteries were reproduced with kind permission from Springer + Business Media: Current Cardiovascular Imaging Reports, "Optical Coherence Tomography in Assessing Plaque Characteristics," 3(4), (2010), 197–206, B.-K. Kim, J.-S. Kim, and M.-K. Hong, Figs. 2, 5, and 6.

References

1. B. W. Pogue and M. S. Patterson, "Review of tissue simulating phantoms for optical spectroscopy, imaging and dosimetry," *J. Biomed. Opt.* **11**(4), 041102 (2006).
2. D. M. de Bruin et al., "Optical phantoms of varying geometry based on thin building blocks with controlled optical properties," *J. Biomed. Opt.* **15**(2), 025001 (2010).
3. P. Urso et al., "Skin and cutaneous melanocytic lesion simulation in biomedical optics with multilayered phantoms," *Phys. Med. Biol.* **52**(10), N229–N239 (2007).
4. R. J. Nordstrom, "The need for validation standards in medical imaging," in *Design and Performance Validation of Phantoms Used in Conjunction with Optical Measurement of Tissue II*, pp. 756702–756707, SPIE, San Francisco, California (2010).
5. G. J. Tearney et al., "Consensus standards for acquisition, measurement, and reporting of intravascular optical coherence tomography studies: a report from the international working group for intravascular optical coherence tomography standardization and validation," *J. Am. Coll. Cardiol.* **59**(12), 1058–1072 (2012).
6. G. Lamouche et al., "Review of tissue simulating phantoms with controllable optical, mechanical and structural properties for use in optical coherence tomography," *Biomed. Opt. Express* **3**(6), 1381–1398 (2012).
7. C.-É. Bisaillon, M. L. Dufour, and G. Lamouche, "Artery phantoms for intravascular optical coherence tomography: healthy arteries," *Biomed. Opt. Express* **2**(9), 2599–2613 (2011).
8. J. M. Schmitt, A. Knuttel, and R. F. Bonner, "Measurement of optical properties of biological tissues by low-coherence reflectometry," *Appl. Opt.* **32**(30), 6032–6042 (1993).
9. A. L. Oldenburg et al., "Magnetomotive contrast for in vivo optical coherence tomography," *Opt. Express* **13**(17), 6597–6614 (2005).
10. G. Lamouche et al., "Intravascular optical coherence tomography on a beating heart model," *J. Biomed. Opt.* **15**(4), 046023 (2010).
11. B.-K. Kim, J.-S. Kim, and M.-K. Hong, "Optical coherence tomography in assessing plaque characteristics," *Curr. Cardiovasc. Imaging Rep.* **3**(4), 197–206 (2010).
12. C. Xu et al., "Characterization of atherosclerosis plaques by measuring both backscattering and attenuation coefficients in optical coherence tomography," *J. Biomed. Opt.* **13**(3), 034003 (2008).
13. G. A. Holzapfel, G. Sommer, and P. Regitnig, "Anisotropic mechanical properties of tissue components in human atherosclerotic plaques," *J. Biomech. Eng.* **126**(5), 657–665 (2004).
14. E. Maher et al., "Tensile and compressive properties of fresh human carotid atherosclerotic plaques," *J. Biomech.* **42**(16), 2760–2767 (2009).
15. N. Gonzalo et al., "Optical coherence tomography patterns of stent restenosis," *Am. Heart J.* **158**(2), 284–293 (2009).
16. F. J. van der Meer et al., "Temperature-dependent optical properties of individual vascular wall components measured by optical coherence tomography," *J. Biomed. Opt.* **11**(4), 041120 (2006).
17. F. J. van der Meer et al., "Quantitative optical coherence tomography of arterial wall components," *Lasers Med. Sci.* **20**(1), 45–51 (2005).
18. G. van Soest et al., "Atherosclerotic tissue characterization in vivo by optical coherence tomography attenuation imaging," *J. Biomed. Opt.* **15**(1), 011105 (2010).